ARTICLE   OPEN

Check for updates

Linkages of unprecedented 2022 Yangtze River Valley heatwaves to Pakistan flood and triple-dip La Niña

Shankai Tang [1,2], Shaobo Qiao [3,4✉], Bin Wang [5], Fei Liu [3,4], Taichen Feng[3,4], Jie Yang[3,4], Meng He[3,4], Dong Chen[3,4], Jianbo Cheng[6], Guolin Feng[1,2,4,7✉] and Wenjie Dong[3,4]

In July-August 2022, Yangtze River Valley (YRV) experienced unprecedented hot summer, with the number of heatwave days exceeding climatology by four standard deviations. The heatwaves and associated severe droughts affected about 38 million people and caused devastating economic losses of about five billion US dollars. Here we present convergent empirical and modelling evidence to show that the record-breaking Pakistan rainfall, along with the 2022 tripe-dip La Niña, produces anomalous high pressure over YRV, causing intense heatwaves. The La Niña-induced second-highest sea surface temperature gradient in the equatorial western Pacific suppresses western Pacific convection and extends the subtropical high westward. More importantly, the tremendous diabatic heating associated with the unprecedented Pakistan rainfall reinforces the downstream Rossby wave train, extending the upper-level South Asia High eastward and controlling the entire YRV. The overlay of the two high-pressure systems sustains sinking motion and increases solar radiation reaching the ground, causing recurrent heat waves.

INTRODUCTION

In recent years, heatwaves have become more frequent and intense over East Asia[1], such as the heatwaves over the Yangtze River valley (YRV) in 2013[2], North China in 2018[3], and South China in 2020[4]. Heatwaves usually concur with high-pressure circulation systems. The induced descending motion leads to decreased cloud cover aloft and increased downward solar radiation at the surface, which favors heatwave occurrence[5,6]. As the major high-pressure system frequently controlling the YRV in midsummer, the western Pacific subtropical High (WPSH) is critical for heatwave formation, especially over its middle and lower reaches[2,7,8]. Moreover, the upper-troposphere South Asia high (SAH) can also strengthen and maintain heatwaves over the YRV by promoting descending motion[9,10]. The westward expansion of the WPSH often accompanies eastward expansion of the SAH. This coupling appears to be caused by the SAH-enhanced middle-lower tropospheric divergence and zonal temperature gradient over subtropical East Asia[11,12].

Previous studies have indicated the roles of tropical sea surface temperature (SST) forcing in modulating the WPSH. The tropical North Atlantic warming may induce a zonally overturning circulation anomaly with anomalous descent over the tropical central Pacific, which acts to enhance the WPSH via triggering a Rossby wave response[13–15]. The Indian Ocean warming emanates the eastward Kelvin waves to the western North Pacific (WNP), which can suppress the convection and enhance the WPSH via the coupled Indo-western Pacific Ocean capacitor[16]. More importantly, the El Niño-Southern Oscillation (ENSO) plays a crucial role in the interannual variations of WPSH through air-sea interactions[17–20]. In particular, Wang et al. (ref. [21]) emphasized two leading modes of low-level WPSH. The first mode is maintained by positive atmosphere-ocean feedbacks with the Indian Ocean warming

and WNP cooling to prolong the effect of the wintertime El Niño[16,17,22], named as an atmosphere-ocean interaction mode[23]. The second mode reflects an enhanced WPSH forced by the summertime La Niña, regarded as a La Niña-forced mode[19,24,25].

Besides the tropical SST forcing, the extratropical atmospheric teleconnections in the mid-upper troposphere originating from North Atlantic and Eurasia can propagate to East Asia and impact the summer climate[15,26–29]. For example, the positive Scandinavian pattern propagates from the Scandinavian Peninsula across Russia to East Asia[30], which leads to high-pressure anomalies and more heatwaves in North China[31]. As for YRV heatwaves, the roles of the Silk Road pattern[32] and the circumglobal teleconnection (CGT) pattern[33] have been highlighted[6,15,31], where the Silk Road pattern is considered to be part of CGT. The CGT is characterized by a wavenumber-5 structure over West Asia, East Asia, North Pacific, North America, and West Europe[33]. The CGT's action center over East Asia can displace the East Asia westerly jet northward, promoting a northeastward extension of the SAH and a westward expansion of the WPSH[8,12,34]. It is widely accepted that the Indian summer monsoon (ISM) rainfall is a key factor in exciting the CGT[33,35,36]. The diabatic heating source released by the anomalous rainfall can excite an upper-level Rossby wave high over central Asia[37,38], enhancing the CGT pattern downstream along the westerly jet-induced waveguide.

In 2022, high-intensity and long-lasting heatwaves hit the YRV in the midsummer (July and August) (Fig. 1a, b). The anomalous surface air temperature (SAT) and heatwave days (HWDs) averaged over the YRV (26°N–34°N/100°E–122°E) have reached 2.42 K and 23.12 days, respectively. The total number of heatwave days exceeds the climatology by four standard deviations (Fig. 1c). According to statistics from the Ministry of Emergency Management of China, the induced drought disasters have affected about

[1]College of Atmospheric Sciences, Lanzhou University, Lanzhou, China. [2]College of Physical Science and Technology, Yangzhou University, Yangzhou, China. [3]School of Atmospheric Sciences, and Key Laboratory of Tropical Atmosphere-Ocean System, Ministry of Education, Sun Yat-sen University, Zhuhai, China. [4]Southern Marine Science and Engineering Guangdong Laboratory (Zhuhai), Zhuhai, China. [5]Department of Atmospheric Sciences and International Pacific Research Center, University of Hawaii at Manoa, Honolulu, USA. [6]School of Environmental Science and Engineering, Yancheng Institute of Technology, Yancheng, China. [7]Laboratory for Climate Studies, National Climate Center, China Meteorological Administration, Beijing, China. ✉email: qiaoshb3@mail.sysu.edu.cn; fenggl@cma.gov.cn
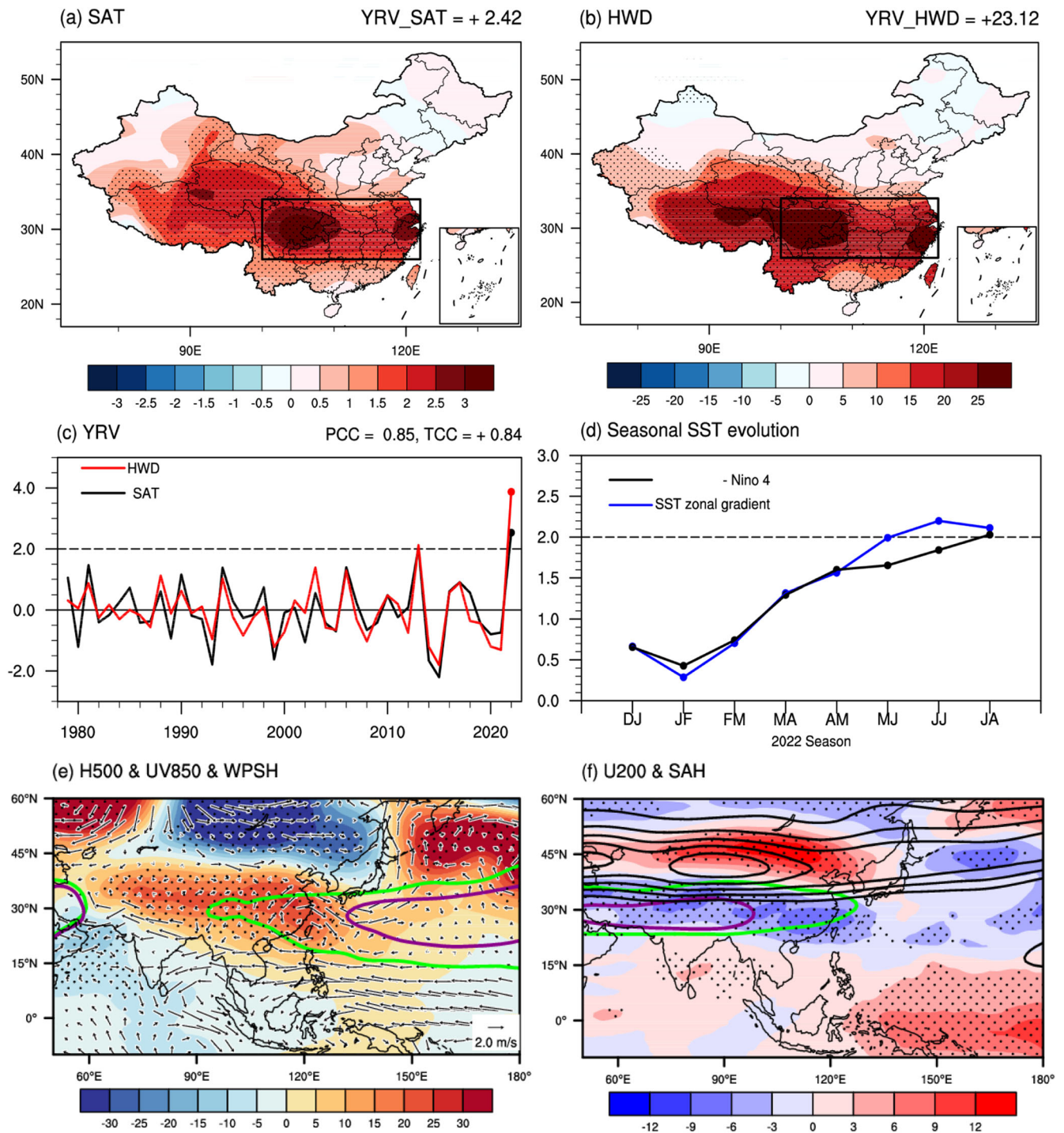
Fig. 1 2022 midsummer (July–August) climate anomalies relative to the 1979–2021 climatology. a surface air temperature (SAT, shading; K) and **b** heatwave days (HWDs, shading; day) anomalies. The black rectangle indicates the Yangtze River valley (YRV) region. Values at the top right of the panels indicate the anomalies averaged over YRV. **c** Standard deviations of the anomalous HWDs (red line) and SAT (black line) averaged over the YRV during 1979–2022. **d** Seasonal evolution of the zonal SST gradient anomaly in the equatorial western Pacific (blue line) and the reversed Niño 4 index (black line) in 2022. The values are normalized by standard deviation. **e** 500-hPa geopotential height (shading; gpm) and 850-hPa wind anomalies (vector; m s^{-1}), and **f** 200-hPa zonal wind anomalies (shading; m s^{-1}) and climatology (black contours at 5, 10, 15, 20 and 25 m s^{-1}). The purple and green lines represent the climatological and 2022 5880-gpm isopleth in **e** and the 12560-gpm isopleth in **f**. Stippling represents the shading values exceeding one standard deviation.

38 million people and caused direct economic losses of 32.8 billion Chinese yuan (https://www.mem.gov.cn/xw/yjglbgzdt/202209/t20220917_422674.shtml). Even if the long-term linear trends are removed, the 2022 midsummer remains to set the hottest record during the 1979–2022 period (Fig. 1c). While we

have a general understanding of the causes of the YRV hot summer, what makes the 2022 unprecedented YRV heatwaves remains a mystery.

This study aims to understand the causes of the record-breaking heatwave days over the YRV in the 2022 midsummer. We find that
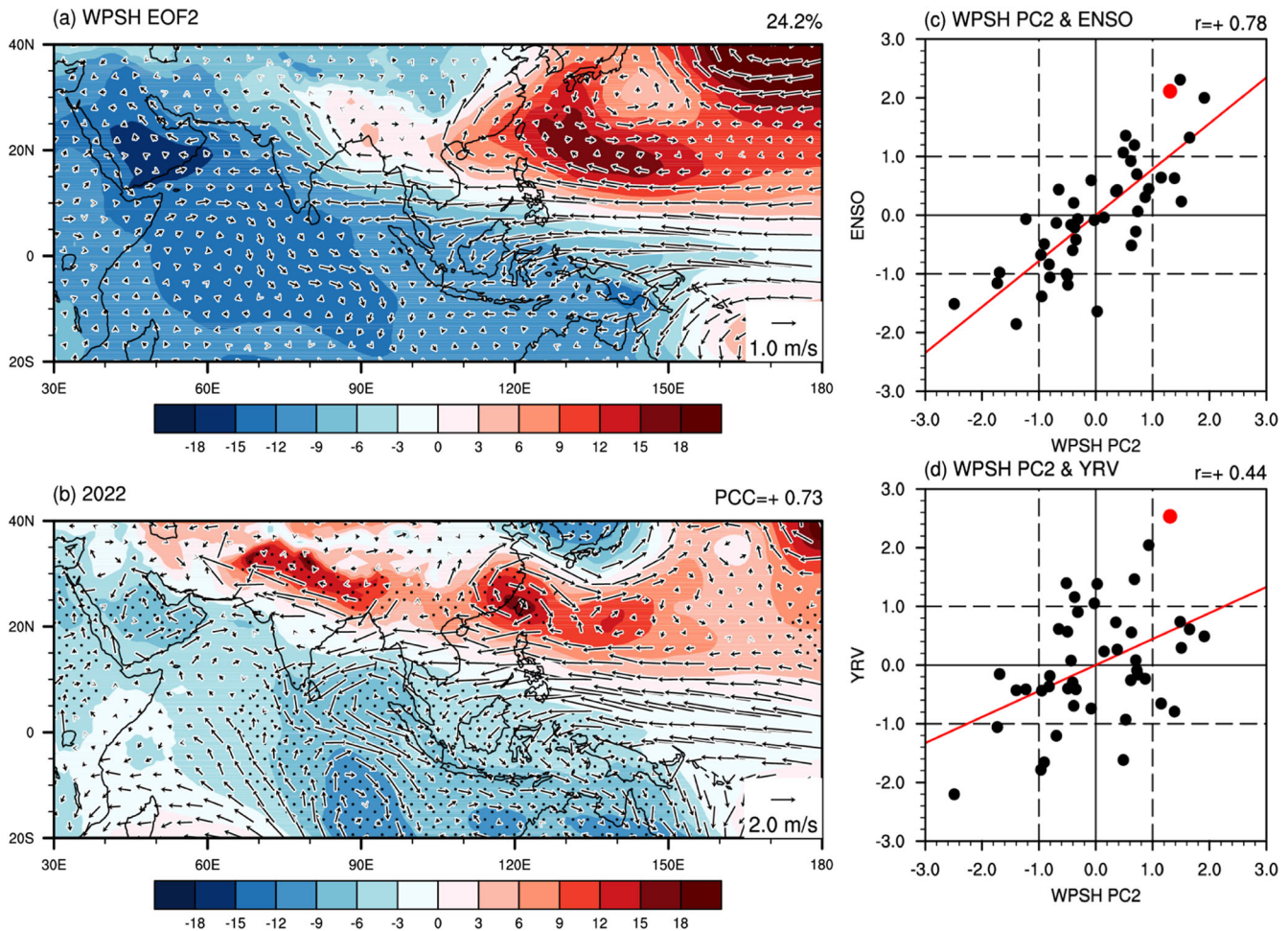
Fig. 2 The La Niña-forced mode of the western Pacific subtropical High (WPSH). a The spatial pattern of the WPSH EOF2 mode (shading) derived from summer-mean 850-hPa geopotential height anomalies in the Asian-Australian monsoon domain (20°S–40°N, 30°E–180°E), and the regressed 850-hPa winds onto the WPSH PC2 (vectors; m s^{-1}). **b** 850-hPa geopotential height (shading; gpm) and wind (vectors; m s^{-1}) anomalies in 2022 midsummer. Stippling represents the shading values exceeding one standard deviation. **c** Scatter plot between the normalized WPSH PC2 and SST zonal gradient in the equatorial western Pacific during the 1979–2022 midsummer. The red dot represents the year 2022. The midsummer intensity of the WPSH PC2 in **c**, **d** is obtained by projecting the midsummer-mean 850-hPa geopotential height anomalies onto the WPSH EOF2 mode. **d** The same as **c**, but for the normalized WPSH PC2 and YRV SAT.

traditional thinking of the role of La Niña cannot explain its extremity, and the unprecedented Pakistan floods play a leading role in generating the 2022 YRV heatwaves. These findings help us understand and predict East Asia's extreme heatwave events.

RESULTS
The associated atmospheric circulation anomalies

A barotropic high-pressure system is the main feature of atmospheric circulation anomalies associated with the 2022 YRV heatwave. The 500-hPa geopotential height shows positive anomalies from the WNP to northern India (Fig. 1e). It indicates an enhanced WPSH with a pronounced westward expansion to the eastern flank of the Tibetan Plateau. The 5880-gpm isopleth extends westward by about 40° of longitude compared to its climatological position (Fig. 1e). The westward expansion of the WPSH is associated with a low-level WNP anticyclone (WNPAC) that controls the middle and lower reaches of the YRV (Fig. 1e). Meanwhile, the westerly winds over mid-latitude Asia are strengthened around 45°N, about 5° to the north of the climatological latitude (Fig. 1f). Correspondingly, the SAH ridge extends eastward from the climatological location of the Tibetan Plateau to the East China Sea around 130°E (Fig. 1f). We

hypothesize that the pronounced westward expansion of the WPSH and eastward stretch of the SAH are the direct causes for this hottest midsummer in the YRV.

The influence of the 2022 triple-dip La Niña

2022 is the third year of a rare three-year La Niña. Usually, ENSO decays from winter to summer. However, the SST anomalies associated with the 2022 La Niña enhanced and extended westward from the preceding winter to the next midsummer, strengthening the zonal SST gradient in the equatorial western Pacific (Fig. 1d; Supplementary Fig. 1). We measure the zonal SST gradient by the SST differences between 5°S–5°N/100°E–140°E and 5°S–5°N/160°E–200°E. The zonal SST gradient in 2022 midsummer exceeds 2.0 standard deviations (Fig. 1d), which is much stronger than 2020 (0.63) and 2021 (0.59) and ranks second since 1979 (Fig. 2c).

The La Niña-forced WPSH anomaly can be represented by the second empirical orthogonal function mode of the summer 850-hPa geopotential height anomalies in the Asian-Pacific domain (20°S–40°N, 30°E–180°E) (Fig. 2a; ref. [21]). The 2022 midsummer 850-hPa geopotential height anomalies display a spatial pattern resembling the La Niña-forced WPSH mode (the pattern correlation coefficient (PCC) is 0.73) (Fig. 2b). We find that the zonal SST

gradient in the equatorial western Pacific is highly correlated with the La Niña-forced WPSH mode with a correlation coefficient of 0.78 ($p < 0.001$) (Fig. 2c), suggesting the influence of the 2022 La Niña on WPSH. Physically, the La Niña-induced zonal SST gradients shift the Walker Circulation westward, suppressing (enhancing) convection over the central equatorial Pacific (Maritime Continent). The anomalous heating associated with these convective anomalies reinforces the low-level WPSH by generating descending Rossby waves over the WNP[10,19].

However, La Niña alone is insufficient to fully explain such extreme 2022 heatwaves. The La Niña-forced WPSH mode was not exceptionally strong, and it covers only the middle and lower reaches of the YRV (Fig. 2a), which cannot explain the high-pressure anomalies over the upper reach of the YRV and the eastern Tibet Plateau in 2022 (Fig. 1e). Besides, the La Niña-forced WPSH mode does not show a strong linkage with YRV heatwaves: The correlation coefficient is merely 0.44 ($p < 0.01$) (Fig. 2d). Therefore, other factors must be in play.

The impacts of the record-breaking Pakistan rainfall

In the 2022 midsummer, Pakistan suffered from unprecedented heavy rainfall and floods[39]. The accumulated rainfall exceeds 500 mm and sets the highest historical record (https://nwfc.pmd.gov.pk/new/monthly-reports.php). The record-breaking Pakistan rainfall could impact the 2022 YRV heatwaves by promoting downstream Rossby wave trains. For this reason, we examined the upper-level circulation anomalies.

In the 2022 midsummer, the upper-troposphere circulation shows an anomalous wave train pattern similar to that associated with YRV heatwaves during the historical period (PCC = 0.80; Fig. 3a vs. b). Both resemble the CGT pattern with positive action centers over West Europe, West Asia, East Asia, and North Pacific (Fig. 3c). These results suggest that the enhanced CGT may play an important role in generating YRV heatwaves during both the historical period and the 2022 midsummer. The enhanced CGT can displace the westerly jet northward and extend the SAH northeastward[8,34,40]. The upper tropospheric high-pressure anomalies associated with the positive CGT action center over East Asia closely link with YRV heatwaves, as evidenced by a correlation coefficient of 0.81 ($p < 0.001$) between them (Supplementary Fig. 2b).

The robust CGT wave pattern is reinforced by Rossby wave responses to the tremendous diabatic heating over Pakistan and northwest India (Fig. 4b), because the ISM rainfall-induced diabatic heating is a key factor in sustaining the summertime CGT[33,36]. Accordingly, we find that the Pakistan rainfall and YRV SAT are well coupled in both the interannual timescale during the historical period (Fig. 4c) and the intraseasonal timescale during the 2022 midsummer (Fig. 4d). The leading singular value decomposition (SVD) mode of the Pakistan rainfall anomalies and East Asia SAT anomalies also validate their close relationship (Supplementary Fig. 3). It is worth noting that the unprecedented Pakistan rainfall that occurred in the 2022 midsummer exceeds climatology by three standard deviations (Fig. 4a, c). Correspondingly, the extreme YRV SAT also exceeds the climatology by 2.5 standard deviations (Fig. 4c).

One might wonder whether the Pakistan flooding is related to the La Nina condition. The linkage between Pakistan rainfall and YRV heatwaves is basically independent of ENSO forcing: the correlation coefficient between them is 0.49 ($p < 0.01$) after removing the effect of ENSO (Supplementary Fig. 4b), just slightly below their original correlation ($r = 0.55$, $p < 0.01$) (Fig. 4c). The regressed CGT pattern onto the Pakistan rainfall with ENSO removed is almost unchanged (Fig. 4b vs. Supplementary Fig. 4a). The structure of 200-hPa geopotential height anomalies associated with La Niña differs from that of 2022 midsummer (PCC = 0.19), especially for the weaker action centers over West

Asia and East Asia (Fig. 3a vs. d). These results indicate that La Niña is unable to explain the enhanced CGT pattern and northeastward stretch of the SAH in 2022 midsummer.

Numerical experiments evidence

We designed sensitivity experiments with the Community Atmospheric Model (CAM) version 6.0 model to assess the respective contributions of the Pakistan rainfall and La Niña (see "Methods" for numerical experiment designs). The ensemble of each experiment minus the ensemble of CTL, denoted as EXP_SST-CTL, EXP_Q-CTL, and EXP_Q_SST-CTL in Fig. 5, represents the model response to La Niña, the Pakistan rainfall, and their combination in 2022 midsummer, respectively. In response to La Niña, the model well reproduces the anomalous WNPAC (Fig. 5a), confirming the mechanism by which La Niña strengthens the low-level WPSH. The Pakistan diabatic heating leads to the CGT action centers over West Asia and East Asia, accompanied by the enhanced SAH and WPSH (Fig. 5e). In both two runs, positive SAT anomalies occur over the YRV under the control of the high-pressure systems (Fig. 5c, f). It is worth noting that the amplitudes of CGT and SAT anomalies in EXP_Q-CTL are relatively stronger than in EXP_SST-CTL, indicating the leading contribution of the Pakistan rainfall in 2022 midsummer. When La Niña and Pakistan rainfall occur together, the CGT, SAH, and WPSH are all further enhanced compared to those when forced by each factor (Fig. 5g, h). Correspondingly, high SAT occurs in a large area from Tibetan Plateau to the YRV exceeding 0.6 K (Fig. 5i). However, the stimulated high-temperature zone in East China has a northward displacement relative to the observation (Fig. 1a). It may be due to the model limitation: The simulated subtropical westerly jet in CTL is significantly northward relative to the observed climatology (Supplementary Fig. 5; ref. [41]).

Moreover, a 1000-year CESM2 pre-industrial (PI) control experiment is conducted to better understand the synchronization among CGT, La Nina, Pakistan rainfall, and YRV heatwaves in a larger-sample and coupled-modelling environment without anthropogenic forcing. The intense Pakistan rainfall is necessary for the formation of the CGT wave train, especially for the East Asia center and heatwaves over the YRV (Supplementary Fig. 6a, d). La Niña alone with normal Pakistan rainfall only forms the zonal symmetric seesaw pattern (Supplementary Fig. 6c), unable to explain such extreme YRV heatwaves (Supplementary Fig. 6e). Above all, these numerical experiments support our hypothesis that the unprecedented Pakistan rainfall played a crucial role in forming the record-breaking heatwaves over the YRV via triggering the intense CGT in 2022 midsummer. In contrast, La Niña helped strengthen YRV heatwaves through enhancing the low-level WPSH.

DISCUSSION

In this study, we present the convergent empirical and modeling evidence to show that the unprecedented Pakistan floods can have a leading contribution to the record-breaking YRV heatwaves in the 2022 midsummer. This finding is beyond the traditional view of the dominant role of La Niña in the YRV heatwave. The specific mechanisms are summarized in the schematic diagram in Fig. 6. The extreme westward expansion of the middle-lower level WPSH and the eastward stretch of the upper-level SAH are responsible for the hottest midsummer of the YRV. On the one hand, the triple-dip La Niña in 2022 exhibits an abnormal enhancement and westward movement from the preceding winter to midsummer. The intensified equatorial western Pacific SST gradient generates descending (ascending) motion and the suppressed (enhanced) convection over the central equatorial Pacific (Maritime Continent), enhancing the WPSH via emanating descending Rossby waves (strengthening the off-equatorial
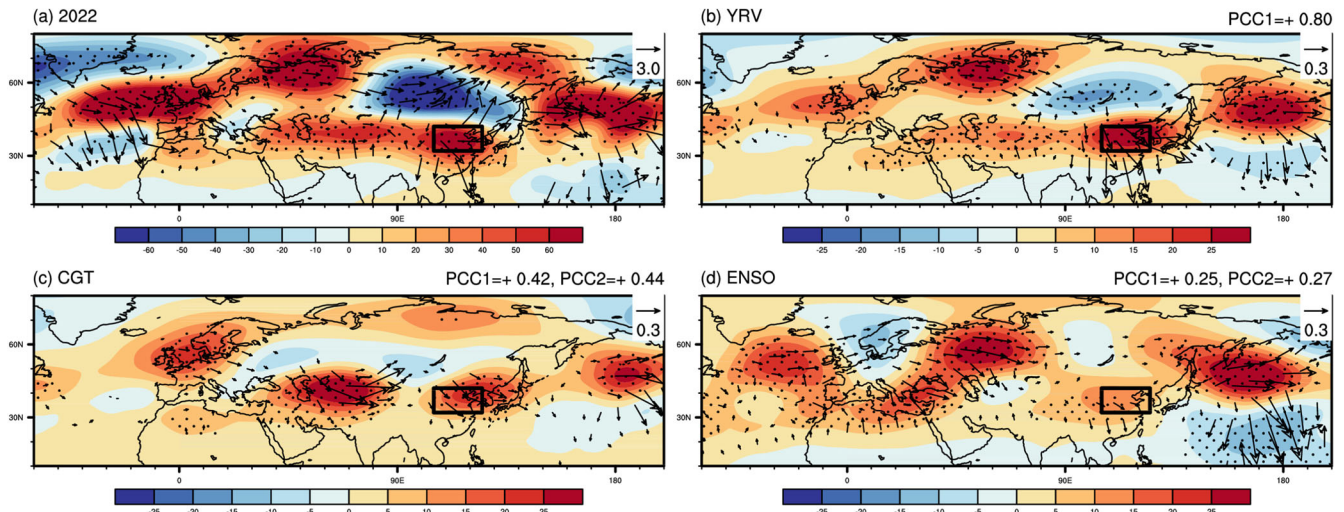
H200 & TN flux

Fig. 3 The midsummer upper-tropospheric Rossby wave trains and associated energy propagation. a 200-hPa geopotential height anomalies (shading; gpm) and the associated horizontal wave activity flux (vector; m^2 s^{-2}) in 2022 midsummer. **b–d** The 200-hPa geopotential height anomalies (shading; gpm) and the associated horizontal wave activity flux (vector; m^2 s^{-2}) regressed onto **b** the YRV surface air temperature (SAT), **c** the circumglobal teleconnection (CGT) index, and **d** the zonal SST gradient in the equatorial western Pacific during 1979–2022. The CGT intensity index is measured by the 200-hPa height anomalies averaged over West Asia (35°N–40°N/60°E–70°E) (Ding & Wang 2005). Stippling shows the 200-hPa geopotential height anomalies exceeding one standard deviation in **a** and significant at the 95% confidence level in **b–d**. PCC1 and PCC2 on **b–d** denote, respectively, their pattern correlation coefficients with the pattern in **a** and **b** over (30°–70°N, 0°–150°E). The black rectangle indicates the CGT action center over East Asia.
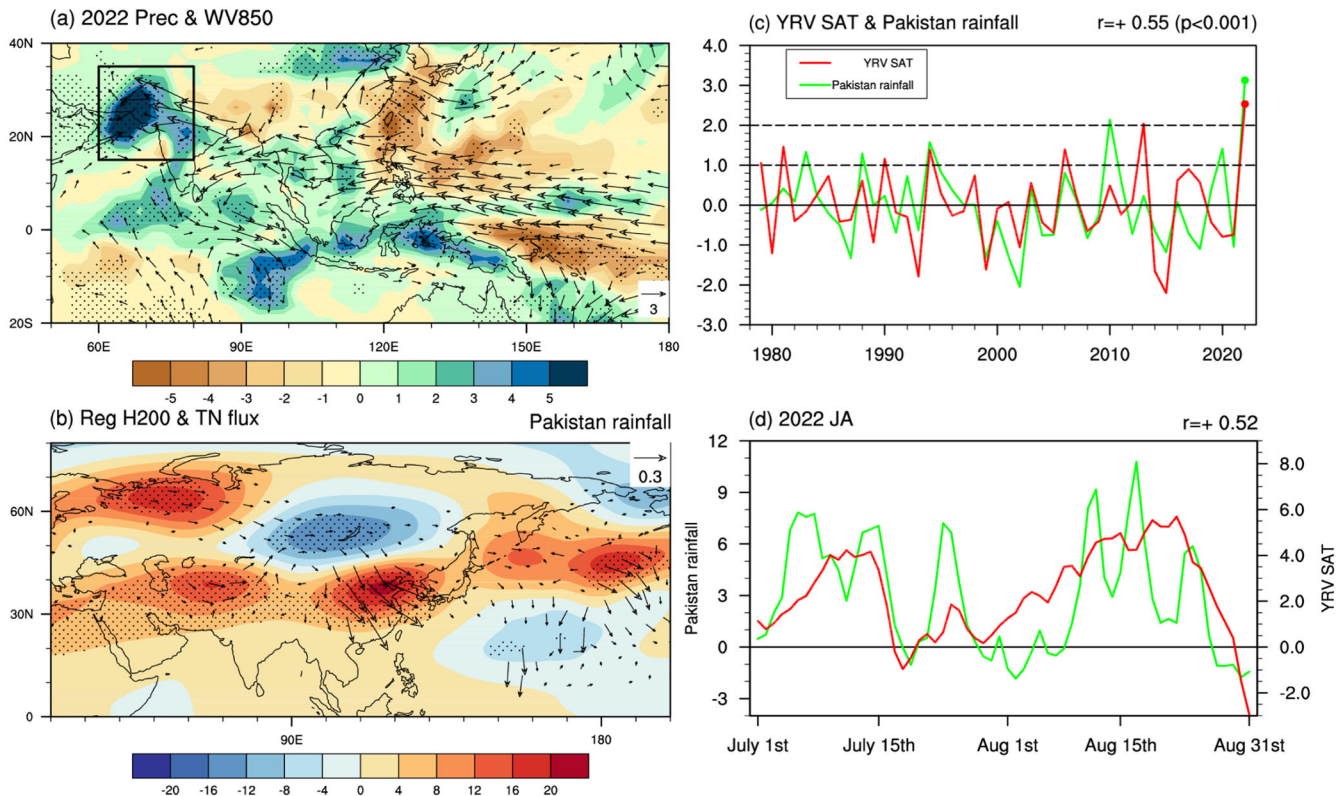

Fig. 4 The linkage between the Yangtze River valley (YRV) surface air temperature (SAT) and Pakistan rainfall averaged over (15°N–35°N, 60°E–80°E). a Rainfall (shading; mm day^{-1}) and 850-hPa moisture flux (vectors; gm^{-1}s^{-1}Pa^{-1}) anomalies in 2022 midsummer. **b** Midsummer 200-hPa geopotential height anomalies (shading; gpm) regressed onto the Pakistan rainfall and the associated horizontal wave activity flux (vector; m^2 s^{-2}) during 1979–2022. Stippling represents 200-hPa geopotential height anomalies exceeding one standard deviation in **a** and the significance at the 95% confidence level in **b**. **c** Normalized midsummer YRV SAT (red line) and the Pakistan rainfall (green line) during 1979–2022. **d** Pakistan rainfall (mm day^{-1}) and YRV SAT (K) anomalies from July 1st to August 31st, 2022.
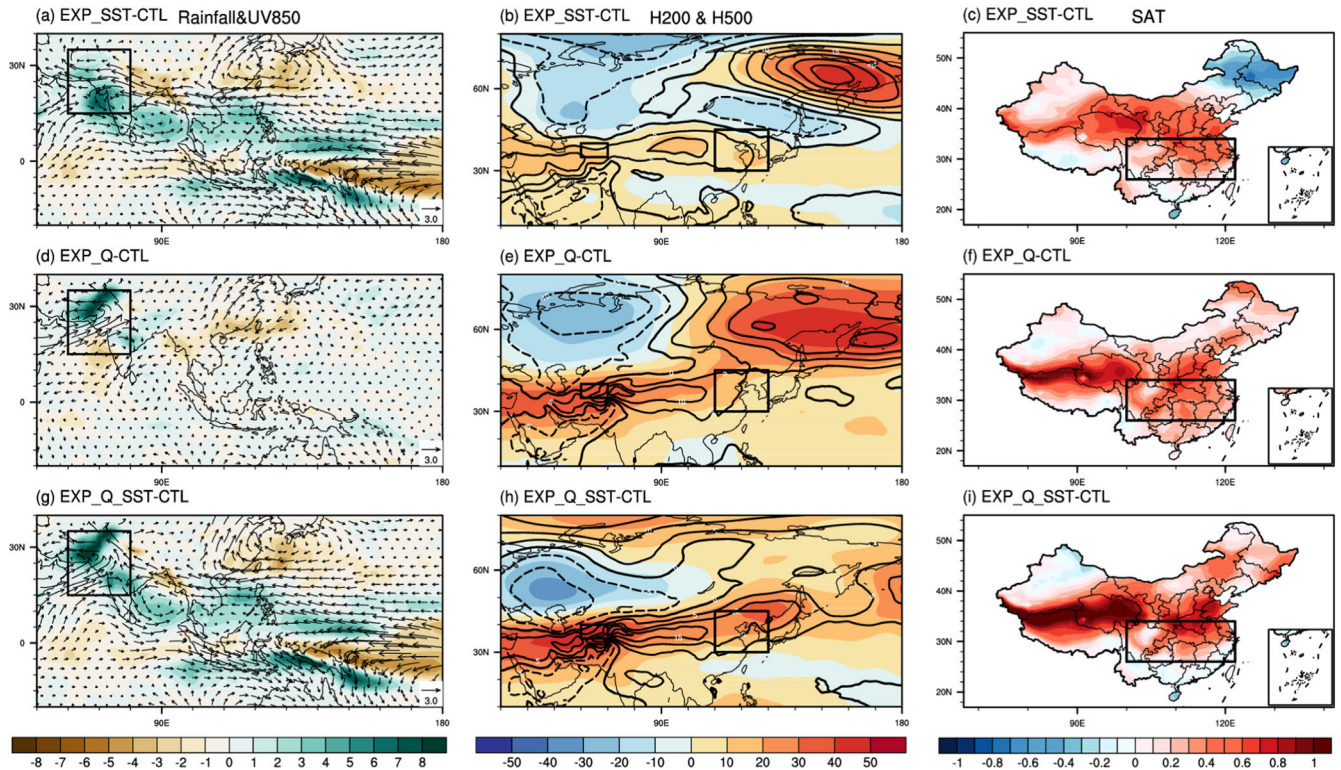
Fig. 5 Numerical experimental results. a Anomalies of rainfall (shading; mm day^{-1}) and 850-hPa winds (vector; m s^{-1}), **b** 200-hPa (shading; gpm) and 500-hPa (contours; Solid line is positive and dashed line is negative with an interval of 5 gpm) geopotential height, and **c** SAT in EXP-SST–CTL. **d–f** and **g–i** The same as in **a–c**, but for EXP_Q–CTL and EXP_Q_SST–CTL, respectively.

anticyclonic shear vorticity) over the WNP. More importantly, the diabatic heating associated with the record-breaking Pakistan rainfall strengthens the upper-level west Asian High center on the CGT and reinforces the downstream East Asia high center extending the upper SAH. Numerical experiments show the leading role of the record-breaking Pakistan rainfall and the contribution of abnormal development of the 2022 La Niña during the midsummer. Additionally, both the observations and sensitivity experiment simulations suggest that the Pakistan rainfall also promotes the Tibetan plateau heatwaves via enhancing the SAH in 2022 midsummer (Fig. 1a, b), which motivates us to investigate the similarities and differences in causes and mechanisms of heatwaves over Tibetan plateau and YRV in the future.

A question arose: why the Pakistan rainfall is so extreme in 2022 midsummer? First, La Niña alone cannot explain such excessive Pakistan rainfall. Most areas of Pakistan belong to the arid region outside the ISM region[42]. The Pakistan rainfall-ENSO relationship is weaker than the ISM-ENSO relationship, which is supported by the numerical experiments (Fig. 5a). Second, positive feedbacks are pronounced between the Pakistan rainfall and CGT[35,36]. The strong barotropic instability at the Atlantic westerly exit provides the upstream disturbances, and strong stationary wave energy is transported from West Europe to West Asia by the Rossby wave train in local basic state. As a result, an anomalous upper-level anticyclone is formed over the northwestern India, which favors Pakistan rainfall through enhancing convection and easterly vertical shear. It is noted that North Atlantic Oscillation (NAO) in 2022 midsummer is intensely positive, the southern center of which is located in the Atlantic westerly exit (Supplementary Fig. 7). The potential impacts of NAO on the interactions between the Pakistan rainfall and CGT should be highlighted[43,44]. Last but not least, such extreme rainfall over Pakistan is associated with enhanced atmospheric river originating from the Arabian Sea[45], which may be the chaotic feature of the climate system. Further
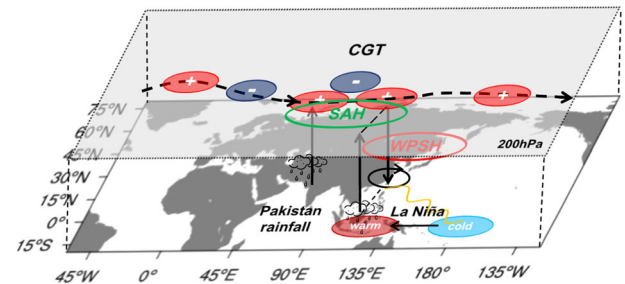

Fig. 6 A schematic diagram illustrating the mechanism of record-breaking YRV heatwaves in 2022 midsummer. The red or blue centers at 200-hPa represent the positive or neagtive CGT centers of action, respectively, and the dotted arrow respresent the westerly jet. The warm and cold centers at surface refer to the equatorial western Pacific SST gradient, and the yellow wavy line refers to the triggerred descending Rossby wave. See the text for details.

work is needed to understand the causes of the extreme Pakistan rainfall fully.

METHODS

Observation data
The observed daily 2-m air temperature data in China are obtained from the 2479 meteorological stations of the China Meteorological Administration for 1951–2022. The daily atmospheric circulation data, including geopotential height and wind, are derived from the European Center for Medium-Range Weather Forecasts Reanalysis 5 (ERA5) at a 0.25° × 0.25° horizontal resolution for 1979–2022[46]. The monthly diabatic heating rates at each level are derived from the Japan Meteorological Agency Reanalysis (JRA-55) diagnostic field dataset with a horizontal resolution of 1.25° × 1.25°

for 1979–2022[47]. The monthly rainfall and SST data are derived from the Global Precipitation Climatology Project (GPCP) v2.3 for 1979–2022[48] and the Extended Reconstructed SST (ERSST) v5 for 1854–2022[49], with a horizontal resolution of $2.5° \times 2.5°$ and $2.0° \times 2.0°$, respectively. The midsummer climate conditions are calculated by the average values of the daily or monthly data during July and August. The anomalies are calculated by the original values minus the climatological mean during the 1979–2021 period. To eliminate the potential influences of global warming, we removed the long-term trends of all datasets.

Heatwaves definition
HWDs are defined as the days when the daily maximum temperature exceeds the 90% threshold of the calendar day based on a 5-day window[50]. Considering that the anomalous SAT and HWDs over the YRV are highly correlated on both the temporal and spatial scales (Fig. 1a–c), the midsummer-mean SAT anomalies are applied to represent the intensity of heatwaves in this study.

Statistical tools and significance
The main statistical tools in this study include the EOF analysis, SVD analysis, correlation analysis and regression analysis. The stationary wave activity flux is calculated to depict Rossby wave propagations[51,52]. The two-tailed Student's t-test with n–2 degrees of freedom (n is the number of years) is applied to examine the statistical significance level for the correlation and regression analysis.

Numerical experiments
The atmosphere component of Community Earth System Model (CESM) v2.1, Community Atmospheric Model version 6.0 (CAM6.0)[53], was used for numerical experiments. The CAM6.0 model is the latest version in a series of global atmosphere models developed primarily by the National Center for Atmospheric Research (NCAR), which have been widely applied in previous research to understand the processes and mechanisms responsible for climate variability and change[54]. All the runs are conducted under a F_2000_climo component set with a horizontal resolution of f09_f09_mg17 (192 × 288 latitudes-longitudes) and 32 vertical levels. Ocean and sea ice were prescribed as the current climatological SST and sea ice.

In the control run (CTL), the model is forced by the model-default climatological-mean monthly SST with a seasonal cycle for 25 years. The last 20 years are used to make an ensemble mean. Based on this, three sensitivity experiments are conducted for additional 20 years. The EXP_SST experiment is forced by the reconstructed SST field by adding the anomalous SST in the tropical western-central Pacific (15°S–15°N,100°E–140°W) in July and August (Supplementary Fig. 8a) to the model-default SST. The EXP_Q experiment is forced by the same SST field as the CTL run, but adding the anomalous diabatic heating rate over Pakistan and northwest India (15°N–35°N, 60°E–80°E) in July and August with a specified vertical heating profile (Supplementary Fig. 8b). We set the anomalous profile below 900-hPa and above 100-hPa zero to eliminate the topographic and stratospheric effects. The diabatic heating rate is the sum of the convective, large-scale condensation, longwave radiative, solar radiative, and vertical diffusion heating rates. The anomalous heating rate at the center is set maximum with the double value of the regional-mean heating rate and linearly decreased to zero at the edges (Supplementary Fig. 8c). The EXP_Q_SST experiment is designed by adding both the two types of forcing in EXP_SST and EXP_Q. The added anomalous SST and diabatic heating rate are multiplied by 1.5 relative to the 2022 midsummer observations, in order to highlight their impacts in the model.

The pre-industrial (PI) control experiment based on CESM v2.1 is fully coupled in all model components with the horizontal resolution of f09_f09_mg17, which is forced by fixed external forcing at 1850 levels and runs freely. In this study, 1000-years PI simulations are applied to assess the contribution of internal climate variability to recent circulation variability without anthropogenic forcing.

REFERENCES
1. Perkins-Kirkpatrick, S. E. & Lewis, S. C. Increasing trends in regional heatwaves. *Nat. Commun.* **11**, 3357 (2020).
2. Sun, Y. et al. Rapid increase in the risk of extreme summer heat in Eastern China. *Nat. Clim. Change* **4**, 1082–1085 (2014).
3. Ding, T., Yuan, Y., Zhang, J. & Gao, H. 2018: The hottest summer in China and possible causes. *J. Meteorol. Res.* **33**, 577–592 (2019).
4. Ye, Y. & Qian, C. Conditional attribution of climate change and atmospheric circulation contributing to the record-breaking precipitation and temperature event of summer 2020 in southern China. *Environ. Res. Lett.* **16**, 044058 (2021).
5. Qian, W. Heat waves and cold events. Temporal Climatology and Anomalous Weather Analysis, *Springer*, 347–423 (2017).
6. Gao, M. et al. Are Peak Summer Sultry Heat Wave Days over the Yangtze-Huaihe River Basin Predictable. *J. Clim.* **31**, 2185–2196 (2018).
7. Wang, B. & Lin, H. Rainy season of the Asian-Pacific summer monsoon. *J. Clim.* **15**, 386–398 (2002).
8. Chen, X. et al. Emergent constraints on future projections of the western North Pacific Subtropical High. *Nat. Commun.* **11**, 2802 (2020).
9. Li, J. et al. Analysis on the extreme heat wave over China around Yangtze River region in the summer of 2013 and its main contributing factors. *Adv. Meteorol. Sci. Tech.* **2015**, 706713 (2015).
10. Wang, W., Zhou, W., Wang, X., Fong, S. & Leong, K. Summer high temperature extremes in Southeast China associated with the East Asian jet stream and circumglobal teleconnection. *J. Geophys. Res.: Atmosph.* **118**, 8306–8319 (2013).
11. Krishnamurti, T. N. et al. Tibetan high and upper tropospheric tropical circulation during northern summer. *Bull. Am. Meteorol. Soc.* **54**, 1234–1250 (1973).
12. Wei, W., Zhang, R., Wen, M., Rong, X. & Li, T. Impact of Indian summer monsoon on the south Asian high and its influence on summer rainfall over China. *Clim. Dyn.* **43**, 1257–1269 (2014).
13. Hong, C., Chang, T. & Hsu, H. Enhanced relationship between the tropical Atlantic SST and the summertime western North Pacific subtropical high after the early 1980s. *J. Geophys. Res.: Atmospheres* **119**, 3715–3722 (2014).
14. Chang, T., Hsu, H. & Hong, C. Enhanced influences of tropical Atlantic SST on WNP–NIO atmosphere–ocean coupling since the early 1980s. *J. Clim.* **29**, 6509–6525 (2016).
15. Li, J., Zheng, F., Sun, C., Feng, J. & Wang, J. Pathways of influence of the Northern hemisphere mid-high latitudes on East Asian climate: a review. *Adv. Atmos. Sci.* **36**, 902–921 (2019).
16. Xie, S. et al. Indian Ocean capacitor effect on Indo-Western Pacific climate during the summer following El Niño. *J. Clim.* **22**, 730–747 (2009).
17. Wang, B., Wu, R. & Fu, X. Pacific-East Asia teleconnection: How does ENSO affect East Asian climate? *J. Clim.* **13**, 1517–1536 (2000).

18. Wu, B. & Zhou, T. Oceanic origin of the interannual and interdecadal variability of the summertime western Pacific subtropical high. *Geophys. Res. Lett.* **35**, L13701 (2008).

19. Wang, B., Li, J. & He, Q. Variable and robust East Asian monsoon rainfall response to El Niño over the past 60 years (1957-2016). *Adv. Atmos. Sci.* **34**, 1235–1248 (2017).

20. Li, T. et al. Theories on formation of an anomalous anticyclone in western North Pacific during El Niño: A review. *J. Meteorol. Res.* **31**, 987–1006 (2017).

21. Wang, B., Xiang, B. Q. & Lee, J. Y. Subtropical high predictability establishes a promising way for monsoon and tropical storm predictions. *Proc. Natl Acad. Sci. USA* **110**, 2718–2722 (2013).

22. Wu, B., Li, T. & Zhou, T. Relative contributions of the Indian Ocean and local SST anomalies to the maintenance of the Western North Pacific anomalous anticyclone during the El Nino decaying summer. *J. Clim.* **23**, 2974–2986 (2010).

23. Huang, Y. et al. Changes in the influence of the western Pacific subtropical high on Asian summer monsoon rainfall in the late 1990s. *Clim. Dyn.* **51**, 443–455 (2018).

24. Chung, P. H., Sui, C.-H. & Li, T. Interannual relationships between the tropical sea surface temperature and summertime subtropical anticyclone over the western North Pacific. *J. Geophys. Res.: Atmospheres* **116**, D13111 (2011).

25. Tang, S. et al. Predictability of the record-breaking rainfall over the Yangtze and Huaihe River valley in 2020 summer by the NCEP CFSv2. *Atmos. Res.* **266**, 105956 (2022).

26. Horton, D. E. et al. Contribution of changes in atmospheric circulation patterns to extreme temperature trends. *Nature* **522**, 465–469 (2015).

27. Schubert, S., Wang, H. & Suarez, M. Warm season sub-seasonal variability and climate extremes in the Northern Hemisphere: The role of stationary Rossby waves. *J. Clim.* **24**, 4773–4792 (2011).

28. Kornhuber, K. et al. Amplified Rossby waves enhance risk of concurrent heat-waves in major breadbasket regions. *Nat. Clim. Chang* **10**, 48–53 (2020).

29. Qiao, S. et al. The longest 2020 Meiyu season over the past 60 years: Subseasonal perspective and its predictions. *Geophys. Res. Lett.* **48**, e2021GL093596 (2021).

30. Bueh, C. & Nakamura, H. Scandinavian pattern and its climatic impact. *Q. J. R. Meteorol. Soc.* **133**, 2117–2131 (2007).

31. Choi, N., Lee, M., Cha, D., Lim, Y. & Kim, K. Decadal changes in the interannual variability of heat waves in east Asia caused by atmospheric teleconnection changes. *J. Clim.* **33**, 1505–1522 (2019).

32. Enomoto, T., Hoskins, B. J. & Matsuda, Y. The formation mechanism of the Bonin high in August. *Q. J. R. Meteorol. Soc.* **129**, 157–178 (2003).

33. Ding, Q. & Wang, B. Circumglobal teleconnection in the Northern Hemisphere summer. *J. Clim.* **20**, 3483–3505 (2005).

34. Liu, G., Wu, R., Sun, S. & Wang, H. Synergistic contribution of precipitation anomalies over northwestern India and the South China Sea to high temperature over the Yangtze River Valley. *Adv. Atmos. Sci.* **32**, 1255–1265 (2015).

35. Ding, Q. & Wang, B. Intraseasonal Teleconnection between the Summer Eurasian Wave Train and the Indian Monsoon. *J. Clim.* **18**, 3483–3505 (2007).

36. Ding, Q. et al. Tropical-extratropical teleconnections in boreal summer: observed interannual variability. *J. Clim.* **24**, 3751–3767 (2011).

37. Gill, A. E. Some simple solutions for heat-induced tropical circulation. *Q. J. R. Meteorol. Soc.* **106**, 447–462 (1980).

38. Wang, Z., Luo, H. & Yang, S. Different mechanisms for the extremely hot central-eastern China in July–August 2022 from a Eurasian large-scale circulation perspective. *Environ. Res. Lett.* **18**, 024023 (2023).

39. He, C. et al. Extremely hot East Asia and flooding western South Asia in the summer of 2022 tied to reversed flow over Tibetan Plateau. *Clim. Dyn.* (2023).

40. Zhou, F., Zhang, R. & Han, J. Influences of the East Asian summer rainfall on circumglobal teleconnection. *J. Clim.* **33**, 5213–5221 (2020).

41. Zhou, Z., Xie, S. & Zhang, R. Historic Yangtze flooding of 2020 tied to extreme Indian ocean conditions. *Proc. Natl Acad. Sci. USA* **118**, e2022255118 (2021).

42. Liu, F. et al. Intraseasonal variability of global land monsoon precipitation and its recent trend. *npj Clim. Atmos. Sci.* **5**, 30 (2022).

43. Branstator, G. Circumglobal teleconnections, the jet stream waveguide, and the North Atlantic Oscillation. *J. Clim.* **15**, 1893–1910 (2002).

44. Watanabe, M. & Jin, F. Dynamical prototype of the arctic oscillation as revealed by aNeutral Singular Vector. *J. Clim.* **17**, 2119–2138 (2004).

45. Nanditha, J. S. et al. The Pakistan flood of August 2022: causes and implications. *Earths Future* **11**, e2022EF003230 (2023).

46. Hersbach, H. et al. The ERA5 global reanalysis. *Q. J. R. Meteorol. Soc.* **146**, 1999–2049 (2020).

47. Kobayashi, S. et al. The JRA-55 reanalysis: general specifications and basic characteristics. *J. Meteorol. Soc. Jpn* **93**, 5–48 (2015).

48. Huffman, G. J. et al. The Global Precipitation Climatology Project (GPCP) Combined Precipitation Dataset. *Bull. Am. Meteorol. Soc.* **78**, 5–20 (1997).

49. Huang, B. et al. Extended reconstructed sea surface temperature, version 5 (ERSSTv5): Upgrades, validations, and intercomparisons. *J. Clim.* **30**, 8179–8205 (2017).

50. Perkins, S. E. & Alexander, L. V. On the measurement of heat waves. *J. Clim.* **26**, 4500–4517 (2013).

51. Takaya, K. & Nakamura, H. A formulation of a wave-activity flux for stationary Rossby waves on a zonally varying basic flow. *Geophys. Res. Lett.* **24**, 2985–2988 (1997).

52. Takaya, K. & Nakamura, H. A formulation of a phase-independent wave activity flux for stationary and migratory quasigeostrophic eddies on a zonally varying basic flow. *J. Atmos. Sci.* **58**, 608–627 (2001).

53. Lauritzen, P. H. et al. NCAR release of CAM-SE in CESM2.0: a reformulation of the spectral element dynamical core in dry-mass vertical coordinates with comprehensive treatment of condensates and energy. *J. Adv. Model Earth Syst.* **10**, 1537–1570 (2018).

54. Danabasoglu, G. et al. The Community Earth System Model Version 2 (CESM2). *J. Adv. Model Earth Syst.* **12**, e2019MS001916 (2020).

AUTHOR CONTRIBUTIONS

S.Q. and G.F. conceived the idea for the study, and S.T. downloaded the data, made the calculations, and created the figures. S.T., J.Y., and S.Q. conducted the experiments. S.T., S.Q., and B.W. wrote the paper. F.L., T.F., M.H., D.C., J.C., and W.D. contributed to the revision. All authors discussed the results throughout the whole process.

COMPETING INTERESTS

The authors declare no competing interests.

ADDITIONAL INFORMATION

Supplementary information The online version contains supplementary material available at https://doi.org/10.1038/s41612-023-00386-3.

Correspondence and requests for materials should be addressed to Shaobo Qiao or Guolin Feng.

Reprints and permission information is available at http://www.nature.com/reprints

Publisher's note Springer Nature remains neutral with regard to jurisdictional claims in published maps and institutional affiliations.